PNAS Nexus, 2023, 2, 1–12
https://doi.org/10.1093/pnasnexus/pgad243
Advance access publication 27 July 2023
Research Report

Titrating CD47 by mismatch CRISPR-interference reveals incomplete repression can eliminate IgG-opsonized tumors but limits induction of antitumor IgG

Brandon H. Hayes [a,b,c,1], Hui Zhu [a,b,1], Jason C. Andrechak [a,b,c], Lawrence J. Dooling [a,b] and Dennis E. Discher [a,b,c,*]

[a]Molecular and Cell Biophysics Lab, University of Pennsylvania, Philadelphia, PA 19104, USA
[b]Physical Sciences Oncology Center at Penn, University of Pennsylvania, Philadelphia, PA 19104, USA
[c]Bioengineering Graduate Group, University of Pennsylvania, Philadelphia, PA 19104, USA
*To whom correspondence should be addressed: Email: discher@seas.upenn.edu
[1]B.H.H. and H.Z. contributed equally to this work.
Edited By: Philip Furmanski

Abstract

Phagocytic elimination of solid tumors by innate immune cells seems attractive for immunotherapy, particularly because of the possibilities for acquired immunity. However, the approach remains challenging, with blockade of the macrophage checkpoint CD47 working in immunodeficient mice and against highly immunogenic tumors but not in the clinic where tumors are poorly immunogenic. Even when mouse tumors of poorly immunogenic B16F10 melanoma are opsonized to drive engulfment with a suitable monoclonal antibody (mAb), anti-CD47 blockade remains insufficient. Using both in vitro immuno-tumoroids and in vivo mouse models, we show with CRISPR interference (CRISPRi) that a relatively uniform minimum repression of CD47 by 80% is needed for phagocytosis to dominate net growth when combined with an otherwise ineffective mAb (anti-Tyrp1). Heterogeneity enriches for CD47-high cells, but mice that eliminate tumors generate prophagocytic IgGs that increase in titer with CD47 repression and with tumor accumulation of macrophages, although deeper repression does not improve survival. Given well-known limitations of antibody permeation into solid tumors, our studies clarify benchmarks for CD47 disruption that should be more clinically feasible and safer but just as effective as complete ablation. Additionally, safe but ineffective opsonization in human melanoma trials suggests that combinations with deep repression of CD47 could prove effective and initiate durable immunity.

Keywords: macrophages, phagocytosis, CD47, titration, antibodies

Significance Statement

Clinical trials show anti-CD47 monotherapy is ineffective against solid tumors. Prior studies in mice show efficacy against highly immunogenic tumors and against tumors in immunodeficient mice. However, in both mouse and human, poorly immunogenic solid tumors remain a challenge even when combining anti-CD47 blockade with monoclonal antibody (mAb) opsonization of cancer cells to drive phagocytosis. Given limits to antibody permeation into solid tumors, CRISPR interference is used to titrate CD47 on poorly immunogenic mouse melanoma to better simulate clinical tumors, showing ~80% repression suffices for eliminating some tumors opsonized by clinically relevant anti-Tyrp1 mAb. Complete repression increases de novo antitumor IgGs, macrophage infiltration, and suppression of heterogeneity, although initial survival remains surprisingly similar. The results also highlight how CD47 heterogeneity modulates acquired immunity.

Introduction

The ubiquitously expressed macrophage checkpoint ligand CD47 is being targeted for cancer therapy, but it is reasonably clear that anti-CD47 monotherapy shows little to no efficacy in patients with solid tumors (1). In lymphoma patients, anti-CD47 combined with anti-CD20 shows some efficacy against these liquid tumors (2). However, with solid tumors, efficient permeation of antibodies is problematic, and even combination treatments such as CD47 blocking antibody magrolimab paired with anti-EGFR cetuximab (Clinical Trial NCT02953782 (3)) have yet to show efficacy (1).

Generally, if a macrophage is stimulated to phagocytose another cell such as by opsonization of the cell by a suitable IgG, then CD47 can act as a "marker of self" to inhibit such phagocytosis. This checkpoint function was first discovered when red blood cells (RBCs) from CD47-deficient C57BL/6 mice were transfused into normal C57BL/6 mice (4). These immunocompetent mice with CD47-knockout exhibit no obvious anemia and display

Competing Interest: The authors declare no competing interest.
Received: December 23, 2022. **Revised:** June 22, 2023. **Accepted:** July 19, 2023

mild phenotypes; furthermore, any factors on the knockout RBCs that stimulate phagocytosis have remained unclear. Intriguingly, immunodefective non-obese diabetic (NON) mice with CD47 knockout are short-lived and develop anemia with anti-RBC IgG (5). The latter observation raises possibilities for prophagocytic IgG subtypes against tumor cells even though CD47 is expressed on all cells, including tumor cells. Perhaps consistent with the single-hit effects in NOD mice, CD47 monotherapy is effective against highly immunogenic solid tumors (6, 7) and also against solid tumors in immunodeficient (8, 9) or immuno-dysfunctional mice (10). However, such reports are now clearly at odds with nearly a decade of clinical results with anti-CD47 in humans (1). Nonimmunogenic tumors in immunocompetent mice treated with well-defined combination therapies clearly require further study, and B16F10 melanoma tumors in C57BL/6 mice provide one such standard model. Although combining anti-CD47 with a long-established prophagocytic monoclonal antibody (mAb) for opsonization is again relatively ineffective against B16F10 tumors (11, 12), alternative approaches seem under-explored, especially for deep repression of CD47.

Antibody permeation into solid tumors can be problematic and frustrate efficacy beyond liquid tumors (13). Any incomplete blockade of CD47 in a solid tumor could enrich for CD47-high cells as a mechanism of "escape" from macrophage-mediated elimination (8, 11). The result would be consistent with the first discovery of CD47 decades ago as highly up-regulated on ovarian cancer cells (as reviewed in Jalil et al. (1)). Furthermore, cancer therapies that target CD47 might also disrupt CD47 on normal cells and lead to safety issues, including anemia and reticulocyte induction in patients (2) or more life-threatening issues (14, 15). Such concerns continue to be raised per a recent FDA hold on anti-CD47 clinical trials because of "suspected unexpected serious adverse reactions" (Clinical Trial NCT04313881 (16)), and the noted emergence of auto-antibodies in NOD mice against RBCs raises broader concerns (5). Hence, from a clinical perspective of balancing efficacy with safety, methods that aim for maximum and complete ablation of CD47 could be less appealing than those that generally seek the "minimum effective dose" (17).

We hypothesized that CRISPR interference (CRISPRi) could be used as a tool to titrate CD47 on B16F10 cells to determine how much repression is needed and how much heterogeneity is tolerated in combination with a clinically relevant opsonizing mAb, anti-Tyrp1 (18). We also hypothesized that induction of de novo antitumor IgG that is prophagocytic would be affected in any surviving mice with different titrated levels of CD47. However, no previous studies have demonstrated whether intermediate levels of CD47 can influence development of IgG or whether such IgG is prophagocytic.

We recently deleted CD47 completely from B16F10 cells and showed increased phagocytosis when paired with anti-Tyrp1 mAb (19), but CRISPRi can tunably repress transcription (20). Additionally, CRISPRi addresses confounding factors with knockouts such as off-target DNA breaks and mutations, CRISPR/Cas9 genotoxicity, expression of oncogenic fusion proteins, and/or dysregulated gene expression (21–28). Furthermore, the CRISPRi approach intrinsically achieves expression heterogeneity that better simulates variations in tumor and antibody therapy. It is well-suited for control of CD47 levels over days and weeks, especially in vivo.

Mismatch CRISPRi ultimately allows us to identify here a critical CD47 density at which therapeutic clearance of tumors by macrophages could be obtained in the clinically relevant context of a syngeneic solid tumor in a fully immunocompetent model. Tumor clearance requires a combination with anti-Tyrp1, but the results show that both CD47 heterogeneity and incomplete repression limit induction of de novo anticancer IgGs that are prophagocytic. High titer might help overcome immune escape and tumor recurrence, but this might only be achievable by better considering CD47 heterogeneity.

Results

Mismatched sgRNAs in CRISPRi titrate CD47 but generate heterogeneity

To identify critical CD47 densities at which phagocytosis starts to show signs of inhibition, we used a recently described CRISPRi method (29) that uses single guide RNAs, sgRNAs, with base pair mismatches to genomic DNA to affect binding of a nuclease dead Cas9 variant (dCas9) (Fig. 1A). We applied our mismatch CRISPRi in the B16F10 mouse melanoma model because it responds poorly to both monotherapy T-cell checkpoint blockade and CD47-SIRPα blockade/disruption in vivo (12). Furthermore, the B16F10 model expresses Tyrp1 antigen, which can be targeted by an existing therapeutic IgG mAb (anti-Tyrp1) that promotes phagocytic uptake by macrophages (18, 19, 30).

First, we identified a base sgRNA (31) that deeply represses CD47 (by 97–99% of original levels) (Fig. S1A and B). While this base sgRNA induces deep repression, we do note that there is still a small subset of cells (~1% of the entire population) that still maintain intermediate-to-high CD47 levels (Fig. 1A, flow cytometry plot insets; Fig. S1A). Nonetheless, the deep repression enables us to systematically perform nucleotide mismatches to greatly alter sgRNA efficacy to generate the desired titration. For choosing mismatches, we assumed that nucleotide position mattered more than the nucleotide itself, based on previous computational modeling experiments (32–34). We then generated an initial compact sgRNA library with mismatches at nearly all nucleotide positions to identify possibly sensitive base sites relative to the protospacer adjacent motif (PAM) (Fig. S1C; Table S1). Like previously reported results (29), we generally found that mismatches near the PAM strongly attenuated sgRNA efficacy, while mismatches in the PAM distal region had little effect. Mismatches in the middle region produced the largest variability of knockdown in terms of repression efficacy and CD47 expression heterogeneity. We thus identified a first set of sgRNAs with mismatches at different nucleotide positions that covered deep, intermediate, and minimal repression of CD47. We then proceeded to generate additional mismatches at these positions to investigate further possible repression levels (Fig. S1D). The final sgRNAs used for subsequent experiments and their resulting CD47 knockdown distributions are shown in Fig. 1B, with sequences for each sgRNA listed in Table S2. We also quantify how many CD47 molecules are presented on each titrated cell lines (Fig. S2) with Table 1 as a control reference, and CD47 expression histograms highlight the percentage of cells in each cell line that have any residual CD47 (Fig. S3). The CRISPRi repression fits well to a sigmoid in terms of a calculated affinity for the targeted sequence (e.g. dCas9-sgRNA to DNA), and the fitted exponent of b is surprisingly high in indicating some mechanism for cooperativity (Fig. 1C). Regardless, the cell-to-cell variation in expression for a given sgRNA is highest in the sigmoid's inflection range, which is consistent with fundamental concepts of susceptibility and binding capacity (Figs. 1C and S4). For example, a cell with the C6A guide that has a small change or difference in sgRNA concentration, will show a large change or difference in CD47 level, and so the sigmoid makes it difficult to fine-tune levels near the EC50.

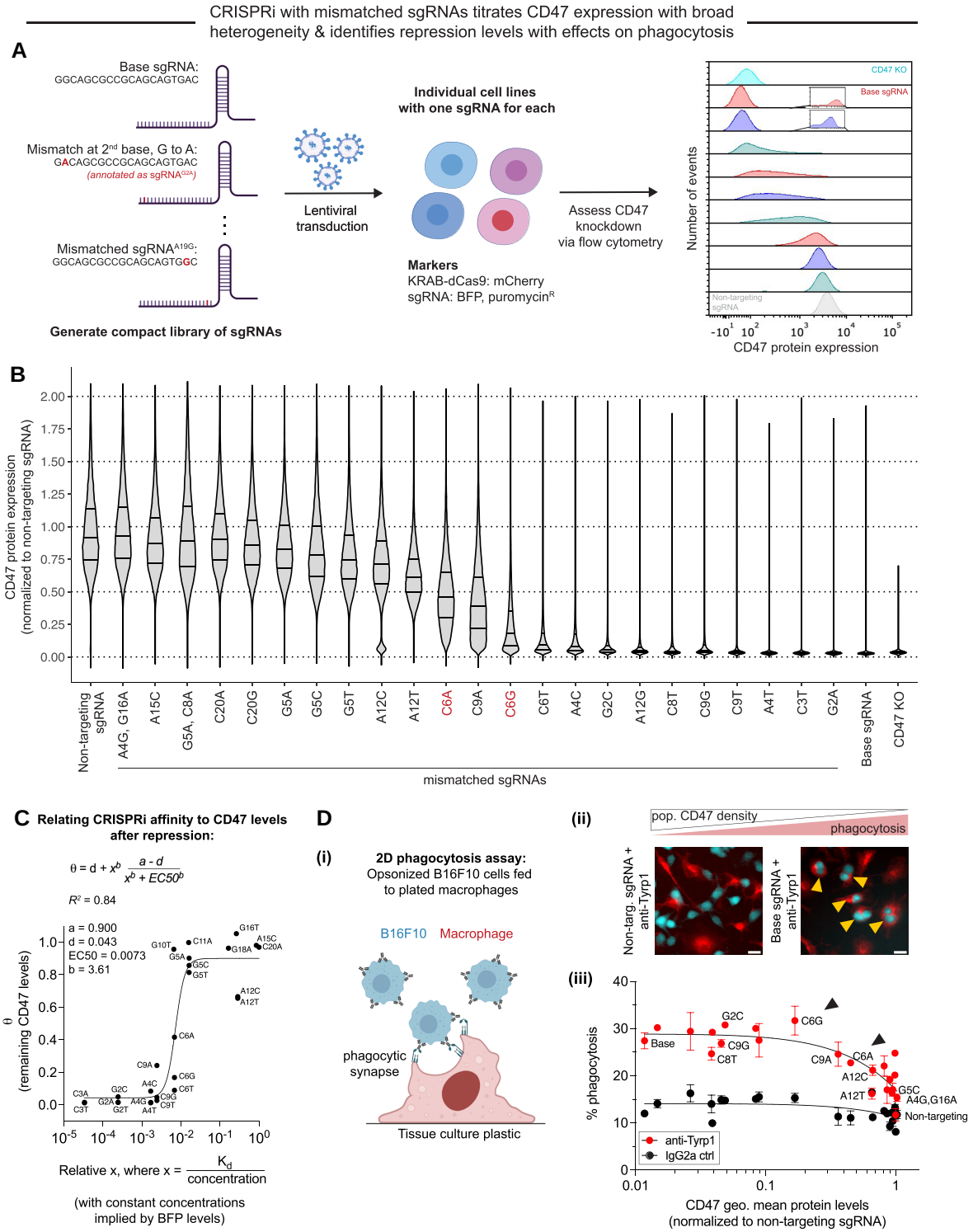

Fig. 1. CRISPRi with mismatched sgRNAs titrates CD47 levels on cancer cells while generating populations with broad CD47 heterogeneity. A) Rational set of mismatched sgRNAs used for CRISPRi based on an initial base sgRNA (31) with one or two base pair mismatches at a position of interest. A single sgRNA packaged into lentivirus was delivered to B16F10 cells followed by antibiotic selection to kill nontransduced cells and CD47 levels measured by flow cytometry. B) Distributions of CD47 levels on B16F10 mouse melanoma cells using a perfectly matched (base) sgRNA, a subset of mismatched sgRNAs, and a nontargeting sgRNA. Additionally, a B16F10 cell line (from the same parental line) with regular CRISPR/Cas9-mediated knockout of CD47 is included for comparisons to complete ablation. All data are obtained by flow cytometry and normalized to the geometric mean CD47 expression of the B16F10 population transduced with the nontargeting sgRNA. sgRNAs C6A and C6G prove to be of greatest interest for in vitro and in vivo studies. C) CD47 levels for tested sgRNAs plotted and fitted against a calculated K_d (32). The same concentration for every sgRNA in every cell was assumed. D) (i) Two-dimensional phagocytosis assay for suspensions of CD47-titrated B16F10 lines added to BMDMs, with or without anti-Tyrp1 for opsonization. (ii) Images are representative of phagocytosis of B16F10 cells with wild-type levels of CD47 (nontargeting sgRNA, left) and deep knockdown (~99% depletion, right). Scale bars = 20 μm. (iii) Quantification of phagocytosis shows that B16F10 cells with ~80% or deeper knockdown of CD47 are phagocytosed maximally when opsonized with IgG, anti-Tyrp1. Arrowheads highlight sgRNAs of greatest interest based in part on differences in phagocytosis efficiency, and the effective inhibition curves (of approximate form $y = a+b/(x^m+k)$) are meant to guide the eye.

Table 1. CD47 surface levels on B16F10 and mouse RBC.

	CD47 molecules per cell
B16 parental (WT)	39,500 ± 1,600
B16 ctrl	40,700 ± 3,800
mouse RBC	10,900 ± 300

WT, wild type.

CD47 titration identifies critical density limits that modulate phagocytosis

We hypothesized that macrophage-mediated phagocytosis of B16F10 would be maximized with the base sgRNA that induces deep CD47 repression and that systematically decreasing sgRNA knockdown efficacy via mismatch CRISPRi would gradually reduce macrophage phagocytic potential. To identify if there are any target cell critical CD47 densities at which this phagocytic activity shows sensitivity to the CD47-SIRPα checkpoint, we first performed conventional 2D phagocytosis assays in which cancer cell suspensions are added to immobilized bone marrow-derived macrophages (BMDMs) (Fig. 1D). Prior to feeding the cancer cell suspension to BMDMs, the B16F10 cells were treated with either anti-Tyrp1 for IgG opsonization to stimulate phagocytosis or mouse IgG2a isotype control. The base sgRNA leads to a ∼2.5-fold increase in phagocytic uptake when B16F10 cells are opsonized with anti-Tyrp1 compared to the mouse IgG2a control. These results are also consistent with previous studies on the importance of opsonizing antibodies that engage Fcγ receptors (35, 36) to ultimately induce a phosphorylation cascade that activates actomyosin tension to facilitate phagocytic internalization (37, 38). We further confirmed that CRISPRi repression did not increase Tyrp1 levels (Fig. S5A–C). SIRPα levels did increase (Fig. S5D and E), consistent with previous studies on CD47-SIRPα *cis* interactions (19) showing that reduced CD47 surface density frees up SIRPα molecules on that same cell surface.

All sgRNAs that repressed CD47 by 80% or more showed nearly identical levels of cancer cell phagocytosis. Once sgRNA knockdown efficacy was less than ∼80%, we observed decreases in macrophage phagocytic ability (Fig. 1D). These reductions in phagocytosis became more drastic as cancer cells had increased CD47 density. These results support the overall hypothesis that macrophages are sensitive to the overall surface density of CD47 molecules on target cancer cells, at least under conditions of constant IgG opsonization, and that tuning these levels yields a distribution of phagocytic activity. Interestingly, the final CD47 surface molecule density that promotes macrophage-mediated phagocytosis of B16F10 here (∼11 CD47 molecules/μm^2) is identical to the number previously found for mouse RBCs that make them more susceptible to macrophage-mediated phagocytosis (∼13 CD47 molecules/μm^2 (37)) (Fig. S2). This similarity further adds confidence to our hypothesis that there is a "critical" threshold that modulates phagocytic activity.

To better model the biophysical properties of the solid tumor microenvironment and the proliferative capacity of tumor masses, we then prepared 3D "tumoroids" of the B16F10 cells in nonadhesive culture plates (Fig. 2A and B). We chose cultures with nontargeting sgRNA (wild-type CD47 levels), base sgRNA (deep repression), and 10 other sublines that covered a broad range of knockdown efficacy and overall heterogeneity for these tumoroid studies. BMDMs were added to preassembled tumoroids at a 3:1 ratio with either anti-Tyrp1 or mouse IgG2a isotype control (Fig. 2C and D). We observed that B16F10 tumoroids with anywhere from 64 to 97% mean CD47 repression were all successfully cleared by macrophages when opsonized with anti-Tyrp1 (Figs. 2C and D and S6A). Knockdown levels of roughly 50% managed to suppress tumoroid growth when opsonized but could not fully clear all tumoroids (Figs. 2C and D and S6B). Knockdown of 35% and lower failed to any tumoroids or even inhibit their growth (Figs. 2C and D and S6C). Altogether, these immuno-tumoroid studies further highlight a critical CD47 surface density and expression heterogeneity at which macrophage-mediated phagocytosis starts to become inhibited. These immuno-tumoroid studies also significantly expand our understanding beyond traditional 2D phagocytosis assays. Pearson correlation analysis between the 2D and 3D result assays shows a strong correlation between both methodologies (Fig. S7), but the 2D phagocytosis assays ultimately fail to capture cancer proliferation effects. 2D assays suggest cells with sgRNA^{C6G} are more susceptible to phagocytosis than their sgRNA^{C6A} counterpart (Fig. 1D-iii), although $P = 0.1255$ via one-way ANOVA. These assays, however, are limited to 2 h only and are suggestive of susceptibility of phagocytosis (but not actual clearance over time). However, 3D tumoroids comprised of sgRNA^{C6G} cells (∼80% repression) were completely cleared, whereas the tumoroids of the sgRNA^{C6A} variant (50% repression) only showed reduced net growth (and 7/8 could not be cleared in this timeframe). This distinction only became clear 48 h after challenging tumoroids with BMDMs (Fig. 2D, right). This was still unclear at 24 h (Fig. 2D, left; the difference between conditions was not statistically significant), a timepoint by which differences could only mostly be attributed to growth suppression. Thus, our immuno-tumoroid assays better capture how high-expressing cancer cells can escape macrophage response.

Significant but incomplete repression of CD47 leads to tumor rejection and de novo IgG

While previous studies (30, 39) show that complete CD47 ablation can favor rejection of IgG-opsonized B16F10 tumors, we sought to find intermediate CD47 expression levels that could yield similar rejection while being more clinically realistic. To select this intermediate CD47-expressing cell line for in vivo tumor models, we performed principal component analysis (PCA) to cluster cell lines with different knockdown levels (different sgRNAs) (Fig. 2E). We considered the following characteristics of each titrated cell line: geometric mean CD47 expression, geometric standard deviation of CD47 expression, overall tumoroid clearance percentage, in vitro tumoroid growth rate (± opsonization), and in vitro 2D phagocytosis percentages (± opsonization). A total of five clusters were determined, of which two were comprised exclusively of B16F10 cell lines that failed to have any 3D tumoroid clearance. We rejected these options since our in vitro studies suggest they would fail to produce durable cures in mice. We then found that B16F10 cell lines with ∼80 and 64% knockdown (sgRNA^{C6G} and sgRNA^{C9A}) uniquely clustered together but separately from the base sgRNA that we intended to use as an in vivo control. Although the B16F10 cell line with sgRNA^{C6A} clustered by itself and showed some degree of tumoroid clearance and growth inhibition (Figs. 2C and S6C), we also rejected it as an in vivo experiment candidate because we wanted to prioritize generating cures in mice. To maximize the possibility of tumor rejection, we chose B16F10 with sgRNA^{C6G} since it had appreciably deep repression and considerable variability in knockdown efficacy (Fig. 1B) and showed complete clearance in 3D tumoroid assays. We also generated a mosaic CD47 knockdown line by mixing B16F10 with sgRNA^{C6G} and sgRNA^{C6A} (Fig. S8). Although repression shows a distribution

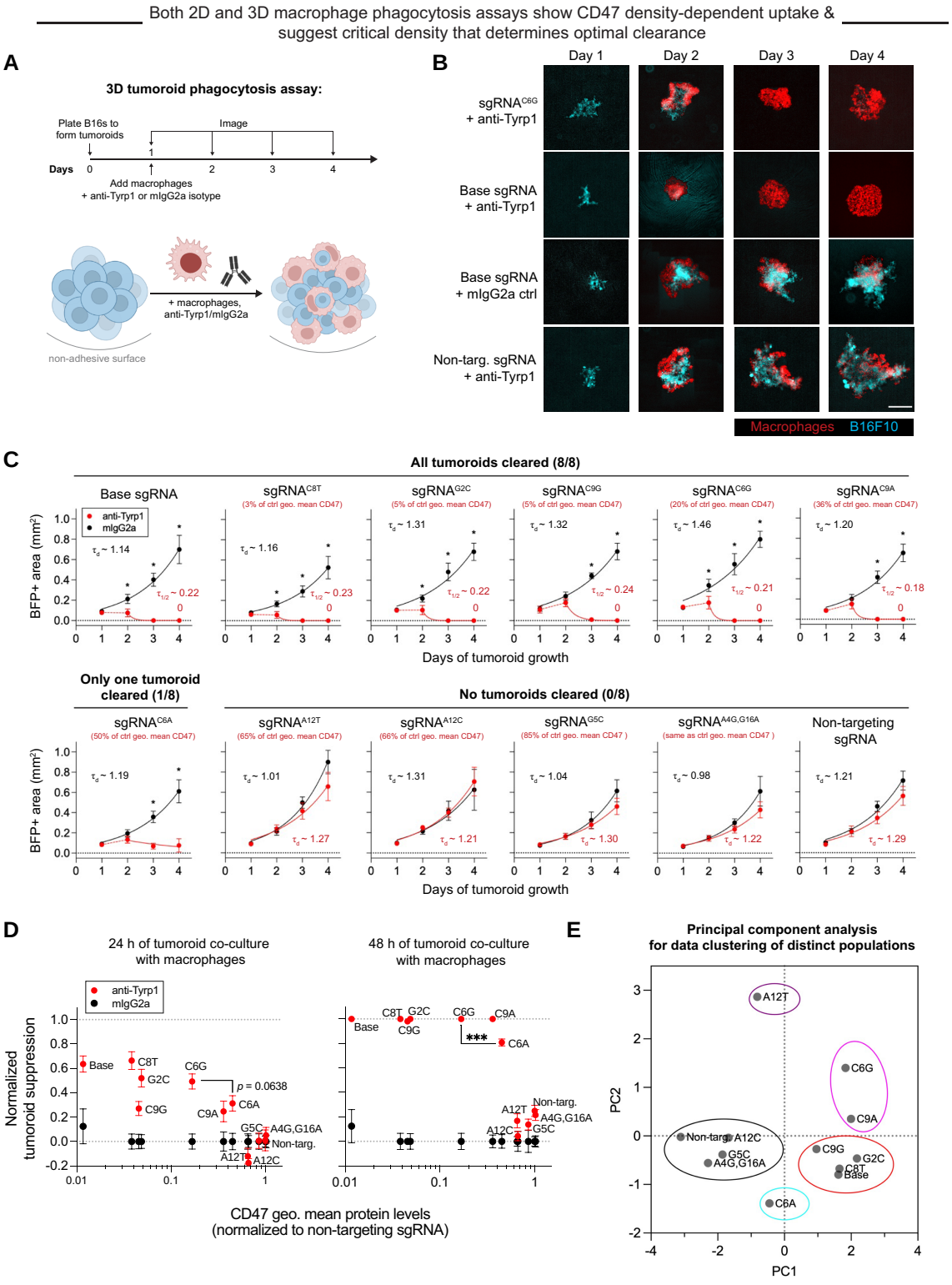

Fig. 2. Major repression of CD47 suffices for macrophage elimination of opsonized tumoroids. A) Timeline and schematic for generating 3D "immuno-tumoroids" of B16F10 cells for macrophage-mediated phagocytosis. B) Fluorescence images of growth or repression of B16F10 tumoroids (light blue: BFP+ from transduction per Fig. 1A). BMDMs, shown in red, were added at a 3:1 ratio to initial B16F10 numbers after the day 1 images were acquired. Scale bar = 0.5 mm. C) Tumoroid size was measured as the BFP+ area (mean ± SD, $n = 8$ total tumoroids from two independent experiments for each sgRNA). Opsonization of B16F10 cells with anti-Tyrp1 eliminates tumoroids only upon depletion of ~64% or more of the original CD47 density (Mann–Whitney *U* test, unpaired, two-tailed, $^*P < 0.05$, at the indicated timepoints). D) Normalized quantification of tumoroid suppression at 24 h (left) or 48 h (right) after addition of macrophages (mean ± SD, $n = 8$ total tumoroids from two independent experiments for each sgRNA). Top dashed line indicates complete suppression, while bottom dashed line indicates no suppressive effect. Statistical significance between tumoroids made of sgRNA^{C6G} and sgRNA^{C6A} (unpaired two-tailed *t*-test with Welch's correction, $^*P < 0.05$). Together, 3D tumoroid and 2D phagocytosis assays suggest that repression of ~64–80% of the original CD47 density levels suffices for therapeutic response when combined with IgG opsonization. E) PCA of the cell lines with the sgRNAs used in all phagocytosis and tumoroid experiments. The following characteristics were used: geometric mean of CD47 expression, geometric standard deviation of CD47 expression, overall tumoroid clearance percentage, in vitro tumoroid growth rate with and without anti-Tyrp1, and in vitro 2D phagocytosis percentages with and without anti-Tyrp1. PCA clusters help select B16F10 lines for more extensive in vivo studies.

of knockdown that includes CD47-intermediate and CD47-high cells, we hypothesized that an existing significant population of CD47-low cells is sufficient to stimulate anticancer macrophage activity that can aid in overall tumor suppression. This mosaic culture allowed us to probe another intermediate CD47-expressing cell line with broad variability while maintaining a significant CD47-low population to potentially activate an immune response.

We proceeded to establish tumors in mice with B16F10 cells with wild-type CD47 levels (nontargeting sgRNA) (Fig. 3A, left), deep repression (base sgRNA) (Fig. 3A, right), and intermediate CD47 expression levels (sgRNA^{C6G} and mosaic) (Fig. 3B). For the wild-type and deep knockdown tumors, we separated mice into groups that received either anti-Tyrp1 opsonizing IgG or mouse IgG2a isotype control. Anti-Tyrp1 treatment seemingly eliminated tumors with deep CD47 knockdown in 23% of mice. Control tumors (including mouse IgG2a-treated deep CD47 knockdown and both anti-Tyrp1-treated and mouse IgG2a-treated wild-type tumors) all exhibited exponential growth and no survivors (Fig. 3A and C). Given that there were no survivors with mouse IgG2a regardless of knockdown level, intermediate CD47-expressing tumors (sgRNA^{C6G} and mosaic) only received anti-Tyrp1. Tumors with sgRNA^{C6G} also resulted in 30% tumor-free mice after 100 days when treated with anti-Tyrp1 (Fig. 3B, bottom), confirming that complete inhibition or ablation of CD47 is not required for tumor rejection. The mosaic tumors, however, all grew exponentially (Fig. 3B, top), suggesting that even with knockdown, CD47 expression heterogeneity is an important factor in tumor rejection and most likely requires a majority of the tumor to be CD47-low.

To further assess how CD47 levels regulate infiltrating macrophage density, we established tumors in mice with B16F10 with wild-type CD47 levels (nontargeting sgRNA), deep repression (base sgRNA), and intermediate CD47 expression levels (sgRNA^{C6G}). These mice were then given one intravenous dose of either anti-Tyrp1 or mouse IgG2a isotype control after 4 days. Mice were sacrificed 24 h later, and tumors were harvested, disaggregated, and stained for flow cytometry measurements of immune cell infiltration (Fig. S9A). We found that the percentage of CD45+ cells in the tumor generally increased with deeper CD47 repression when opsonized, both with and without anti-Tyrp1 (Fig. S9B). However, significantly higher CD45+ infiltration was observed with both intermediate and deep repression compared to the wild-type CD47-expressing cells, when opsonized with anti-Tyrp1. Interestingly, there is no statistically significant difference in CD45+ immune infiltrate between the intermediate and deep repression conditions, which reflects the similar in vivo cure rates observed in Fig. 3C. The percentages of macrophages, however, that made up the myeloid compartment were not different across different levels of repression (Fig. S9C). Opsonization seemed to be the only driving force for increasing the macrophage composition of the myeloid compartment. However, when accounting for the CD45+ immune infiltrate numbers and the overall macrophage percentage of the entire myeloid compartment with anti-Tyrp1, we overall find an increasing number of tumor-infiltrating macrophages with deeper CD47 repression (Fig. S9D). There is a statistically significant difference between no repression and deep repression. We did not attain statistical significance between no repression and intermediate repression, but the reported P-value of 0.134 seems to suggest a possible trend of gradually increasing macrophage numbers with deeper CD47 repression. Lastly, we sought to see what fraction of these macrophages showed M1-like polarization with the commonly used marker CD86. We find that even without opsonization, CD86+ macrophages make up a significant and substantially larger percentage of the macrophage population in both intermediate and deep repression conditions compared to the no repression control (Fig. S9E). This also holds true with opsonization. Lastly, we find that the number of CD86+ macrophages relative to all tumor-harvested cells also increased with both intermediate and deep repression compared to the no repression control (Fig. S9F). We further find that both the percentage (Fig. S9E) and relative number of CD86+ macrophages (Fig. S9F) in both the intermediate and deep repression conditions are nearly equivalent, again reiterating the similarities in in vivo cure rates previously mentioned (Fig. 3C). Altogether, these results suggest that macrophages are key effector cells in rejecting initial tumor engraftment when CD47 is depleted and when tumors are IgG-opsonized. A role for macrophages is also consistent with a survival requirement for IgG opsonization (via anti-Tyrp1) even with very deep CD47 repression (Fig. 3A–C); macrophages are among the few immune cell types that express IgG engaging, Fc receptors that initiate a phagocytic response.

We then proceeded to collect convalescent serum from survivors to quantify de novo anticancer IgG potentially generated via acquired immunity. Sera were collected at the earliest 80 days after the initial challenge and were used in antibody binding and 2D phagocytosis assays (Fig. 3D). We first quantified IgG titer in convalescent sera, focusing on IgG2a and IgG2b, which have been found to engage mouse macrophage Fcγ receptors (40, 41). B16F10 cells, either Tyrp1 expresing or Tyrp1 knockout, were incubated with sera (convalescent from survivors or naïve from unchallenged mice) and then counterstained with conjugated antibodies against IgG2a/c and IgG2b (Fig. 3E). We found that surviving mice showed significant increases in IgG2a binding in both Tyrp1-positive and Tyrp1 KO B16F10 cells. A similar trend was seen in IgG2b binding, although to a much lesser extent. Interestingly though, we find that survivors from deep CD47 knockdown tumors have much higher IgG2a titer than their ~80% repression (sgRNA^{C6G}) counterparts. To test where these de novo serum antibodies functionally promote phagocytosis, we performed conventional 2D phagocytosis assays in which cancer cell suspensions were opsonized with sera (or anti-Tyrp1 or mouse IgG2a as controls) (Fig. 3F). Cells expressing both CD47 and Tyrp1 were poorly engulfed despite opsonization with sera or anti-Tyrp1, consistent with the overall inhibitory effect of CD47 on macrophage-mediated phagocytosis. However, under conditions of maximal phagocytosis (CD47 repression and IgG opsonization by either anti-Tyrp1 or sera), we see that unpurified sera from survivors functionally promote phagocytosis equivalently to anti-Tyrp1 (~4- to 5-fold higher than baseline). We further find that sera continue to promote phagocytosis even in the absence of Tyrp1 in B16F10 CD47/Tyrp1 double knockout cells (~3-fold higher than baseline), suggesting potent acquired immunity with de novo IgG antibodies that target B16F10 antigens beyond Tyrp1.

Mismatch CRISPRi titration captures selection of CD47-positive cells in tumor evolution

Given that CRISPRi does not completely repress CD47 and typically generates expression heterogeneity, we sought to understand how tumor evolution favors CD47-positive cells. In tumors with broadly varying levels of CD47 between cells, macrophages can effectively clear low expressors but allow high expressors to escape (8), thereby creating an opportunity for new cancer populations to emerge. We used both in vitro tumoroids

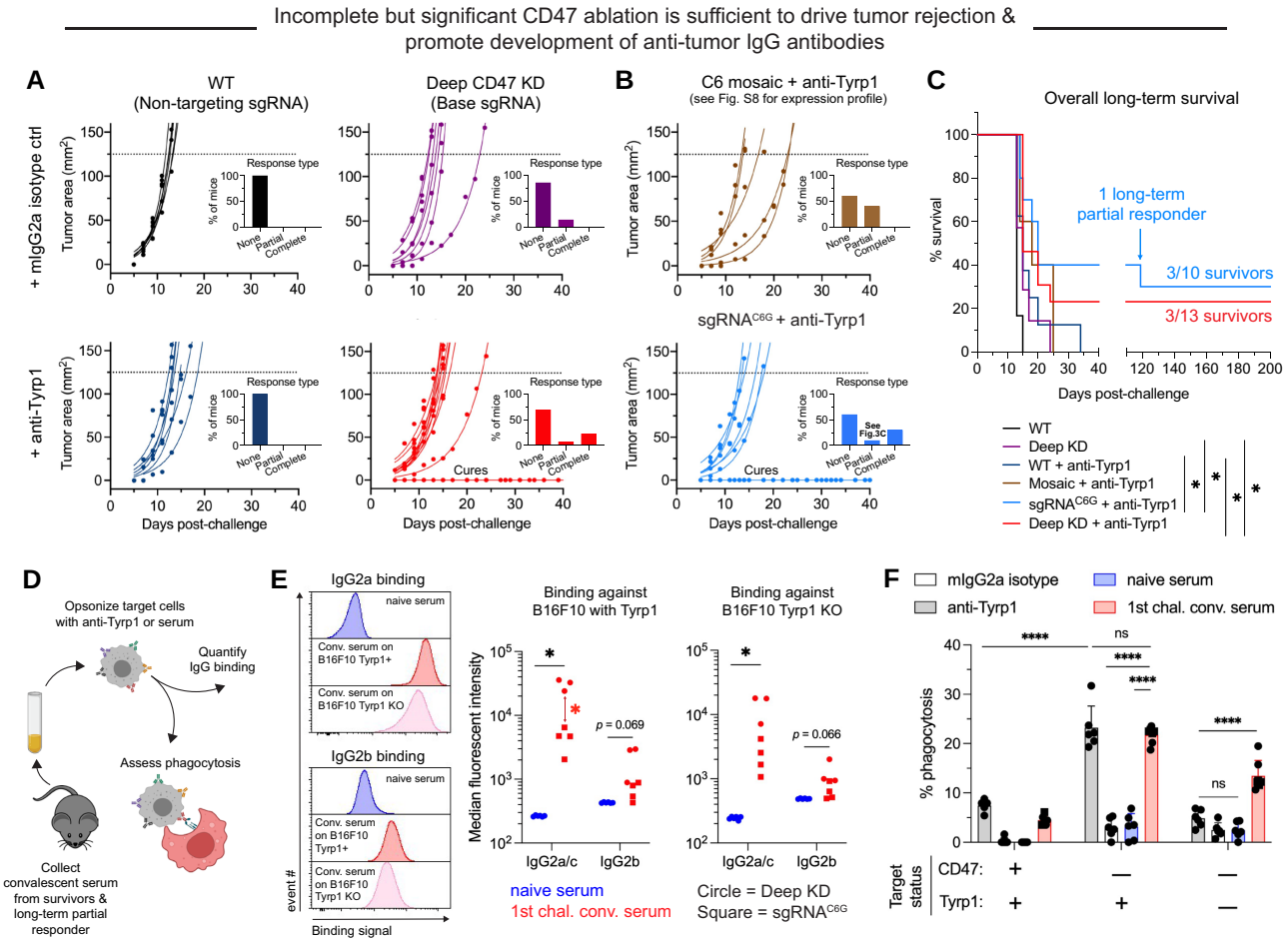

Fig. 3. CD47 suppression to a critical density or lower can eliminate syngeneic tumors in immunocompetent mice and lead to prophagocytic, antitumor antibodies. A) Tumor growth curves for 2×10^5 B16F10 cells expressing wild-type (WT) levels of CD47 or deep knockdown (base sgRNA). Each subcutaneous tumor area is fit with an exponential, $A = A_0 e^{kt}$, and tumors that never grew are shown as solid lines at $A = 0$. Tumors of B16F10 with nontargeting sgRNA: six mice were injected with mouse IgG2a isotype control, and eight mice with anti-Tyrp1. Tumors of B16F10 with the base sgRNA giving deep CD47 knockdown: seven mice were injected with mouse IgG2a isotype control, and 13 mice with anti-Tyrp1. Mice were treated either intravenously or intraperitoneally with 250 μg with anti-Tyrp1 on days 4, 5, 7, 9, 11, 13, and 15 after tumor challenge, across three independent experiments. Inset bar graphs depict response type: a partial response is defined as a mouse that survived 1 week beyond the median survival of the CD47 deep KD cohort without anti-Tyrp1 (20+ days). B) Tumor growth curves for B16F10 cells with titrated levels of CD47 or broad heterogeneity, with fits and bar graphs per panel (A). Ten mice were challenged with B16F10 with sgRNA^{C6G} (bottom), and five mice were challenged with a mosaic B16F10 tumor (top) giving intermediate levels and broad heterogeneity. All mice received anti-Tyrp1 because deep CD47 knockdown showed no survivors when treated with mouse IgG2a isotype control. All data were collected across two to three independent experiments. C) Survival curves of mice up to 100 days after tumor challenges in panels A) and B) (log-rank, Mantel–Cox test, $^*P < 0.05$). D) Schematic protocol for sera collection from surviving mice panels A) and C) and follow-up characterization of de novo anticancer IgG antibodies. E) (Left) Representative flow cytometry histograms of IgG2a/c and IgG2b from convalescent sera (collected 80–105 days postchallenge) binding to wild-type (WT) and to Tyrp1 knockout B16F10 cells that suggests broader recognition of antigens. (Right) Median fluorescent intensity of IgG2a/c and IgG2b from all surviving mice (unpaired two-tailed *t*-test, Welch's correction, $^*P < 0.05$). F) Phagocytosis of serum-opsonized WT, CD47 deep knockdown or CD47/Tyrp1 double knockout B16F10 cells when added to BMDMs on 2D tissue culture plastic. B16F10 cells treated with anti-Tyrp1, mouse IgG2a, or naïve serum were opsonization controls. Note that convalescent sera IgG can drive engulfment of Tyrp1 knockout cells. Circles indicate sera from survivors challenged with B16F10 with base sgRNA (deep repression); squares indicate survivors from challenges with B16F10 with sgRNA^{C6G} (two-way ANOVA, Tukey's multiple comparison test between selected groups: mean ± SD, $n = 7$ distinct serum samples from survivors, $n = 6$ for nonconvalescent serum controls).

(Fig. 4A-i) and tumors from nonsurvivors in tumor challenge experiments (Fig. 4A-ii) to assess how CD47 population expression changes in macrophage-stimulated conditions. After 4 days of coculture with BMDMs and treatment with anti-Tyrp1, tumoroids showed statistically significant upward shifts in the overall population's CD47 expression compared to concurrent B16F10-only tumoroid cultures (Fig. 4B), suggesting that macrophages clear cells with lower CD47 expression, while higher expressors can continue to proliferate. We further found that tumor-derived populations also have more CD47-positive cells compared to their passage-matched in vitro control cultures (Figs. 4C and D and S10). This was true for both tumors with sgRNA^{C6G} (~80% repression) and tumors with base sgRNA (deep repression), although this enrichment was only statistically significant for tumor-derived cultures from tumors with deep CD47 repression. Flow-activated cell sorting (FACS)-isolated CD47-high cells from these tumor-derived cultures were also more resistant to phagocytic uptake compared to in vitro deep knockdown controls in conventional 2D macrophage phagocytosis assays (Fig. 4E), confirming therapeutically unfavorable functional consequences of a tumor population's overall CD47 recovery.

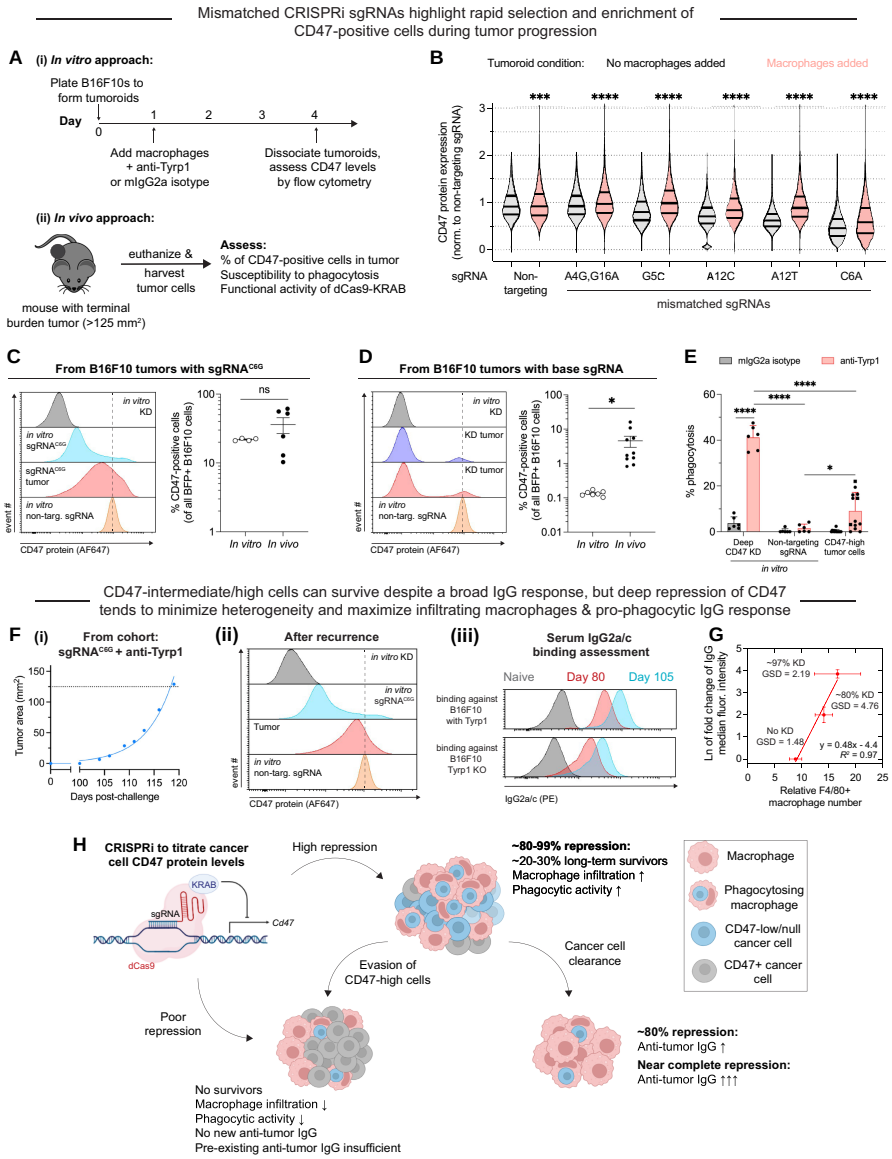

Fig. 4. Tumor evolution favors selection and enrichment of CD47-positive cells and can favor recurrence despite acquired immunity. A) (i) Timeline for measuring changes in population CD47 levels in engineered immuno-tumoroids. B16F10 tumoroids were started, and macrophages were added 24 h later at a 3:1 ratio to initial B16F10 number, with or without anti-Tyrp1. At 72 h after macrophage addition, tumoroids were collected and dissociated for flow cytometry analysis. Concurrently, B16F10 tumoroids with the same sgRNAs but without the addition of macrophages were maintained as a control group. (ii) Timeline for measuring changes in CD47 levels in syngeneic tumors in C57BL/6 mice. Tumors grew to a terminal burden (~125 mm^2), after which mice were humanely euthanized, and tumors were excised and dissociated for flow cytometry analysis and for generating tumor-derived B16F10 cultures for further assays. B) CD47 distributions in immuno-tumoroids at day 4 assessing the effects of added macrophages. Data are normalized to the geometric mean CD47 expression of the concurrent day-matched control tumoroid (no macrophages added, B16F10 cells with nontargeting sgRNA) (Mann–Whitney *U* test, unpaired, two-tailed, $^{***}P < 0.001$, $^{****}P < 0.0001$). C) and D) Flow cytometry histograms of CD47 levels on B16F10 cells harvested from terminal burden tumors in Fig. 3A–C. Dashed lines indicate geometric means of nontargeting sgRNA control. Mean ± SEM for $n = 6$ tumors of B16F10 cells with $sgRNA^{C6G}$ and four passage-matched in vitro cultures of B16F10 with $sgRNA^{C6G}$; $n = 10$ tumors generated from B16F10 cells with base sgRNA and seven passage-matched in vitro cultures of B16F10 with base sgRNA (unpaired two-tailed *t*-test with Welch's correction: ns, not significant, or $^{*}P < 0.05$). E) Phagocytosis of B16F10 with nontargeting sgRNA or base sgRNA (for deep CD47 knockdown) and FACS-sorted CD47-high B16F10 cells isolated from tumor-derived cultures in panels C) and D). The 2D phagocytosis assay was done with BMDMs, with or without anti-Tyrp1 opsonization. For CD47-high tumor cells, circles indicate B16F10 cells FACS-sorted from tumors with base sgRNA, and squares indicate cells from tumors with $sgRNA^{C6G}$. Although tumor-derived CD47-high B16F10 cultures are more readily phagocytosed than in vitro B16F10 with nontargeting sgRNA, they are phagocytosed less than B16F10 with deep CD47 knockdown (mean ± SD shown, $n = 6$ cultures for both deep CD47 knockdown and nontargeting sgRNA, $n = 13$ tumor-derived cultures for CD47-high cells; two-way ANOVA and Tukey's multiple comparison test between selected groups: $^{*}P < 0.05$; $^{****}P < 0.0001$). F) Late cancer recurrence in a mouse from the initial 100-day survivors from the $sgRNA^{C6G}$ cohort. (i) Tumor growth in a mouse with cancer recurrence 104 days after the initial challenge and despite anticancer IgG antibodies. The solid line is $A = A_0e^{kt}$. (ii) Flow cytometry histograms for CD47 protein levels on B16F10 cells harvested from the recurrent tumor. CD47 levels were benchmarked against in vitro B16F10 cells with: base sgRNA (deep CD47 knockdown), $sgRNA^{C6G}$, and nontargeting sgRNA. (iii) Flow cytometry histograms show IgG2a/c and IgG2b from convalescent sera of mouse with recurrent tumor still binds to both wild-type (WT) and Tyrp1 knockout B16F10 cells. Sera were collected before (day 80) and after recurrence (day 105). G) Overall prophagocytic IgG binding signal (IgG2a/c + IgG2b, normalized to values from naïve sera control) for each sgRNA that produced long-term survivors plotted against the relative number of tumor-infiltrating macrophages. Anti-Tyrp1 treatment conditions for macrophage infiltrate used, from Fig. S9D; all data are originally normalized to macrophage numbers from B16F10 tumors with nontargeting sgRNA treated with mouse IgG2a isotype control. Knockdown levels and geometric SD for each cell line are listed next to their respective data point. H) Summary of findings and proposed CD47-dependent effects on tumor evolution and titer of de novo anticancer antibodies.

We further confirmed that these tumor-derived cultures still expressed targetable Tyrp1 antigen (Fig. S11A) and that any variability in Tyrp1 expression correlated weakly with the bimodal engulfment behavior observed (Fig. S11B). Lastly, we confirmed that KRAB-dCas9 in these tumor-derived cultures was still able to induce deep knockdown (using a Tyrp1-targeting sgRNA for quality control assessment), leading us to conclude that decreased functional activity of the KRAB-dCas9 was unlikely (Fig. S11C).

Interestingly, we observed that one mouse from the sgRNA^{C6G} tumor challenge cohort developed a tumor at day 105 (Fig. 4F-i). We isolated convalescent sera from this partial responder at this timepoint and again when terminal burden was reached. We harvested the tumor and then assessed the tumor population's CD47 levels compared to relevant passage-matched in vitro controls (Fig. 4F-ii). We found that the resulting tumor cells were mostly CD47-high expressors, which illustrates how even a few phagocytosis-resistant cancer cells can ultimately drive fatal recurrence. Recurrence occurred despite the generation of phagocytosis-promoting anticancer IgG antibodies. In fact, IgG2a in particular saw significant increases in titer between day 84 (before recurrence) and day 105 (after recurrence) (Fig. 4F-ii).

We consequently reevaluated the observation that deep CD47 repression produced the highest prophagocytic IgG titer (Fig. 3E). Similarly, tumor-infiltrating macrophage numbers also increases with deeper CD47 repression (Fig. S9D). We also see an increase in M1-like, CD86+ macrophages infiltration (Fig. S9E and F). The correlation between these two parameters suggests that prophagocytic IgG titer increases with higher macrophage numbers, which ultimately depends on cancer cell CD47 levels (Fig. 4G) that also relate to heterogeneity in levels (Fig. S3). This analysis thus suggests that deep but incomplete disruption of the CD47-SIRPα checkpoint or CD47 expression heterogeneity is sufficient to inhibit overall immune response and dampen acquired immunity.

Discussion

Clinically, anti-CD47 approaches have shown some degree of efficacy in combination therapies against liquid tumors such as lymphoma (2), but solid tumors have remained problematic (1). This limited success can in part be attributed to better antibody permeation into liquid cancer microenvironments. Anti-CD47 permeation of solid tumors remains a challenge (11), and poor permeation favors selection of CD47-high cancer cells (8). Complete inhibition or knockout in all tumor cells is generally not feasible in the clinic due to both low permeation and in vivo gene-editing challenges (11, 13). CRISPR-based knockout (19, 30, 39) fails to model heterogeneous levels of CD47 among tumor cells, especially in an anti-CD47 blockade context. Heterogeneity favors immune escape of CD47-high cells (Fig. 4B, D, and F-ii) and cancer recurrence. Our results for poorly immunogenic tumors in immunocompetent mice extend previous work on various immunogenic tumors in immunodeficient mice but clearly show that efficacy requires a combination of prophagocytic mAb, major repression of CD47 but not elimination, and low CD47 heterogeneity. These are all needed to overcome cancer cell proliferation and generate cures. Antitumor IgG that develops can then drive further phagocytosis. Such an acquired immune response had not been previously reported in a cancer context, and the findings can potentially translate to treatments for intractable melanoma and might be generalizable to other solid tumors.

Importantly, 80% repression of CD47 when paired with IgG mAb opsonization suffices to yield the same ~30% survival as very deep repression (Fig. 3C), which makes 80% an important therapeutic goal that is likely to be more feasible and safer than complete ablation in terms of off-target effects. The 80% repression still generates antitumor immunity with surviving mice producing intermediate levels of de novo prophagocytic IgGs against B16F10 cells compared to deep repression (Fig. 4G). Auto-immunity against off-target, normal cells seems less likely for human therapies that target ~80% suppression. This is because in the many studies of RBCs from diverse human patients (e.g. Rh blood group deficiency), we had identified what seems to be a tolerable minimum of ~90% reduction of CD47 relative to the average normal (37). RBCs are much smaller than B16F10 cells, and a 90% reduction of CD47 density on mouse RBC (Fig. S2) is nearly equal to an 80% reduction of CD47 density on B16F10 cells. The similar survival here for 80% repression on B16 cells as very deep repression is also surprising because the former shows far greater tumor heterogeneity (Figs. 1A and B and S2–S4). Antitumor IgG provides one signature of acquired immunity, consistent with lysate-based vaccinations with CD47-deficient tumor cells (42); such IgG could even drive phagocytic feedback, which is important because little to no induction might allow even a few CD47-high expressors to proliferate and drive recurrence (Fig. 4B–D, F, and H). A CD47 "threshold" for tumor treatment will thus need to consider heterogeneity as well as mean repression and any anticancer IgG induction—especially for long-term therapeutic outcomes.

One notable recent study using standard 2D phagocytosis assays (Fig. 1D) concluded that the ratio of prophagocytic IgG to inhibitory CD47 expressed on the cancer cell governs phagocytosis efficiency (38). However, opsonization is constant across our in vitro and in vivo studies, and so similar levels of 2D phagocytosis for >97% repression ("base") versus ~80% and even ~65% repression (C6G and C9A, respectively, in Fig. 1D-iii) seem to differ from the noted ratio effects (38). Our 3D immuno-tumoroid studies confirm and extend our simpler 2D results by accounting for effects of tumor growth relative to phagocytosis rate and tumor cell cohesion (Fig. 2D). Our findings also introduce the importance of CD47 expression heterogeneity in determining phagocytosis, and our in vivo studies extend prior findings in showing effects of progressively suppressing CD47 levels, increasing numbers of tumor-infiltrating macrophages, survival beyond a threshold, and induction of de novo IgG. Future studies should of course vary the anti-Tyrp1 prophagocytic mAb among our different CD47-titrated lines and perhaps clarify whether less opsonization is needed for elimination of deep repression versus the ~80% threshold.

Altogether, these data suggest that ~80% depletion or inhibition of CD47 is sufficient to lead to favorable therapeutic outcomes against the poorly immunogenic B16F10 melanoma. Incomplete blockade or inhibition comes with a trade-off—reduced induction of humoral immunity. Nonetheless, cures are comparable to complete ablation (Fig. 3C) and still generate anticancer IgG (Figs. 3E and F and 4G). Anti-CD47 therapies have a history of toxicities, such as anemia (2, 14), some of which have been life-threatening (15). There is a need to determine a "minimum effective dosage" that can achieve therapeutic benefits while minimizing toxicity and side effects (17). This is becoming particularly clear for T-cell checkpoint immunotherapies (43, 44) that increasingly become a main tool in treating cancers. Here, we report a minimum effective inhibition of CD47 that yields favorable outcomes and that could potentially be explored in the clinic to mitigate such safety concerns.

We note, however, different tumor types likely show different CD47 expression levels, and this needs to be considered when

attempting to translate the 80% threshold from the B16F10 melanoma to other tumors. This becomes a more delicate matter when further translating to actual human tumors, such as those registered in The Cancer Genome Atlas (TCGA). Toward this end, we estimated CD47 protein levels based on RNA levels of B16F10 and other tumor types (Fig. S12). In other words, tumor types with more or less CD47 RNA (suitably normalized to housekeeping gene *HSP90AB1* or total RNA) will tend to have more or less CD47 protein. We also indicate for each cancer the percent suppression of CD47 needed to achieve the threshold number of CD47 molecules per cell based on B16F10 results presented here. Human melanoma tumors, based on these estimates, require ∼86% CD47 suppression to achieve therapeutic efficacy, which is similar to the experimentally determined 80% in this study. Remarkably, for all cancers, the RNA-based estimate of CD47 molecules per cell considerably exceeds the "80%" threshold of ∼8,000 molecules per cell determined for B16F10. There is no a priori reason for such a result, but it is consistent with the idea that all cancers have more than enough CD47 to signal "self" to macrophages. Moreover, cancer of the testis shows the minimum level of suppression for efficacy (∼80% suppression needed), consistent again with a large excess of "self" signaling even for this cancer. Such minimum levels of suppression also need to be achieved uniformly in the tumor and combined with opsonization for efficacy, which are additional challenges, and yet deeper suppression should confer a more effective anticancer immune response.

Limitations of the study

Our findings pinpoint an interesting critical CD47 regime that allows macrophages to dominate tumor proliferation, while also highlighting the importance of single-cell CD47 expression heterogeneity in final therapeutic outcomes. We limited our studies to the challenging immunocompetent B16F10 melanoma model because this cell line expresses a well-targeted Tyrp1 antigen for IgG opsonization to stimulate macrophage-mediated phagocytosis (18, 19, 30, 39). Other poorly immunogenic cancer cell lines typically do not have well-characterized mAbs that function in opsonization, which hinders efforts to perform studies combining IgG opsonization with CD47 disruption. B16F10 is also unaffected by CD47 disruption (19), consistent with CD47 monotherapy showing no clinical efficacy against solid tumors (1, 14). Other common syngeneic models, such as MC38 and CT26 colon cancers, respond to CD47 monotherapy independent of macrophages (6, 7), but such lines are more immunogenic compared to B16F10 melanoma (45). It remains to be tested whether CD47 heterogeneity is more important in cancers with fewer presentable neoantigens compared to those that are highly immunogenic.

Lastly, B cells are undoubtedly required for induction of antitumor IgG here in C57BL/6 mice and anti-RBC IgG against CD47-null red cells in NOD mice (5). Although effects related to the immunodeficiency of NOD mice remain unclear in the latter study, macrophages in the spleen phagocytose CD47-null red cells (4), with recent studies establishing their essential role (46) in inducing splenic B cells to make anti-RBC IgG (47). Local tertiary lymphoid structures in human melanoma and other solid tumors have likewise been reported together with local antibody responses (48), and macrophages can serve as antigen-presenting cells in such contexts (49). Related innate immune myeloid cells including dendritic cells have likely roles, which motivates continued study of mechanisms by which IgG are eventually induced in contexts of CD47 disruption. It is an important issue given the anticancer utility of prophagocytic IgG such as anti-Tyrp1 when also suppressing CD47.

Materials and methods

Detailed descriptions are provided in the Supplementary material. Briefly, B16F10 cells (CRL-6475) obtained from American Type Culture Collection (ATCC) were transduced with different sgRNA oligonucleotides packaged and delivered by *Lentivirus*, and this was followed by selection and measurement of CRISPRi-mediated knockdown of CD47. Flow cytometry analyses of anti-CD47 binding levels provided a snapshot of the full distribution of CD47 display, and opsonization for phagocytosis of B16F10 cells made use of antimouse/antihuman Tyrp1 clone TA99 (BioXCell BE0151). In vitro phagocytosis studies made use of Macrophage colony stimulating factor (M-CSF) differentiated BMDMs from 6- to 12-week-old C57BL/6 mice (Jackson Laboratory 000664) with all protocols in accordance with protocols approved by the Institutional Animal Care and Use Committee (IACUC) of the University of Pennsylvania. Tumoroids of B16F10 cells with various surface levels of CD47 were made and imaged for growth in nonadherent 96-well U-bottom plates for multiple days starting with ∼1k B16F10 cells, and one subcutaneous tumor per mouse was made with ∼200k B16F10 cells and palpated for the projected area. Anticancer IgG in the serum of mice that survived tumor challenge was collected and assayed for binding titer to B16F10 cells and for effects in phagocytosis assays.

Acknowledgments

The authors acknowledge the following University of Pennsylvania core facilities: Cell Center Stockroom, the Penn Cytomics and Cell Sorting Resource Laboratory (supported by the Abramson Cancer Center NIH/NCI Grant P30 CA016520), and the Penn Genomic Analysis Core.

Supplementary material

Supplementary material is available at *PNAS Nexus* online.

Funding

This work was supported by funding from the following sources: NIH U01CA254886 (D.E.D.), R01 HL124106 (D.E.D.), NSF GRFP DGE-1845298 (B.H.H. and J.C.A.), and NIH F32 CA228285 (L.J.D.).

Author contributions

Conceptualization: B.H.H., H.Z., L.J.D., and D.E.D. Formal analysis: B.H.H., H.Z., and D.E.D. Funding acquisition: B.H.H., J.C.A., L.J.D., and D.E.D. Investigation: B.H.H. and H.Z. Methodology: B.H.H., H.Z., J.C.A., and L.J.D. Resources: D.E.D. Visualization: B.H.H. and H.Z. Writing: B.H.H., H.Z., and D.E.D.

Data availability

All data are available within the article and its supplementary material.

References

1 Jalil AR, Andrechak JC, Discher DE. 2020. Macrophage checkpoint blockade: results from initial clinical trials, binding analyses,

and CD47-SIRPα structure–function. *Antibody Therapeutics* 3: 80–94.
2 Advani R, *et al.* 2018. CD47 blockade by Hu5F9-G4 and rituximab in non-Hodgkin's lymphoma. *N Engl J Med*. 379:1711–1721.
3 Gilead Sciences, Study of Magrolimab (Hu5F9-G4) in Combination With Cetuximab in Participants With Solid Tumors and Advanced Colorectal Cancer. 2021. (accessed 2022 December 22).
4 Oldenborg P-A, *et al.* 2000. Role of CD47 as a marker of self on red blood cells. *Science* 288:2051–2054.
5 Oldenborg P-A. 2002. Lethal autoimmune hemolytic anemia in CD47-deficient nonobese diabetic (NOD) mice. *Blood* 99:3500–3504.
6 Liu X, *et al.* 2015. CD47 Blockade triggers T cell–mediated destruction of immunogenic tumors. *Nat Med*. 21:1209–1215.
7 Xu MM, *et al.* 2017. Dendritic cells but not macrophages sense tumor mitochondrial DNA for cross-priming through signal regulatory protein α signaling. *Immunity* 47:363–373.e5.
8 Jaiswal S, *et al.* 2009. CD47 Is upregulated on circulating hematopoietic stem cells and leukemia cells to avoid phagocytosis. *Cell* 138:271–285.
9 Willingham SB, *et al.* 2012. The CD47-signal regulatory protein alpha (SIRPa) interaction is a therapeutic target for human solid tumors. *Proc Natl Acad Sci U S A*. 109:6662–6667.
10 Theruvath J, *et al.* 2022. Anti-GD2 synergizes with CD47 blockade to mediate tumor eradication. *Nat Med*. 28:333–344.
11 Ingram JR, *et al.* 2017. Localized CD47 blockade enhances immunotherapy for murine melanoma. *Proc Natl Acad Sci U S A*. 114:10184–10189.
12 Sockolosky JT, *et al.* 2016. Durable antitumor responses to CD47 blockade require adaptive immune stimulation. *Proc Natl Acad Sci U S A*. 113:E2646–E2654.
13 Nia HT, Munn LL, Jain RK. 2020. Physical traits of cancer. *Science* 370:eaaz0868.
14 Horrigan SK. 2017. Reproducibility project: cancer biology, replication study: the CD47-signal regulatory protein alpha (SIRPa) interaction is a therapeutic target for human solid tumors. *eLife* 6:e18173.
15 Li Y, *et al.* 2018. Balancing the efficacy and toxicity of anti-CD47 antibodies by direct screening in humanized mouse models. *Ann Oncol*. 29:x35.
16 Gilead Sciences, Magrolimab + Azacitidine Versus Azacitidine + Placebo in Untreated Participants With Myelodysplastic Syndrome (MDS) (ENHANCE). 2023. (June 15, 2023).
17 Tsatsakis AM, *et al.* 2018. The dose response principle from philosophy to modern toxicology: the impact of ancient philosophy and medicine in modern toxicology science. *Toxicol Rep*. 5: 1107–1113.
18 Khalil DN, *et al.* 2016. An open-label, dose–escalation phase I study of anti-TYRP1 monoclonal antibody IMC-20D7S for patients with relapsed or refractory melanoma. *Clin Cancer Res*. 22:5204–5210.
19 Hayes BH, *et al.* 2020. Macrophages show higher levels of engulfment after disruption of *cis* interactions between CD47 and the checkpoint receptor SIRPα. *J Cell Sci*. 133:jcs237800.
20 Gilbert LA, *et al.* 2014. Genome-scale CRISPR-mediated control of gene repression and activation. *Cell* 159:647–661.
21 Azangou-Khyavy M, *et al.* 2020. CRISPR/Cas: from tumor gene editing to T cell-based immunotherapy of cancer. *Front Immunol*. 11: 2062.
22 Cullot G, *et al.* 2019. CRISPR-Cas9 genome editing induces megabase-scale chromosomal truncations. *Nat Commun*. 10:1136.
23 Kosicki M, Tomberg K, Bradley A. 2018. Repair of double-strand breaks induced by CRISPR–Cas9 leads to large deletions and complex rearrangements. *Nat Biotechnol*. 36:765–771.
24 Leibowitz ML, *et al.* 2021. Chromothripsis as an on-target consequence of CRISPR–Cas9 genome editing. *Nat Genet*. 53:895–905.
25 Lino CA, Harper JC, Carney JP, Timlin JA. 2018. Delivering CRISPR: a review of the challenges and approaches. *Drug Deliv*. 25: 1234–1257.
26 Mout R, Ray M, Lee Y-W, Scaletti F, Rotello VM. 2017. In vivo delivery of CRISPR/Cas9 for therapeutic gene editing: progress and challenges. *Bioconjugate Chem*. 28:880–884.
27 Wilbie D, Walther J, Mastrobattista E. 2019. Delivery aspects of CRISPR/Cas for in vivo genome editing. *Acc Chem Res*. 52: 1555–1564.
28 You L, *et al.* 2019. Advancements and obstacles of CRISPR-Cas9 technology in translational research. *Mol Ther Methods Clin Dev*. 13:359–370.
29 Jost M, *et al.* 2020. Titrating gene expression using libraries of systematically attenuated CRISPR guide RNAs. *Nat Biotechnol*. 38: 355–364.
30 Andrechak JC, *et al.* 2022. CD47-SIRPα checkpoint disruption in metastases requires tumor-targeting antibody for molecular and engineered macrophage therapies. *Cancers (Basel)* 14:1930.
31 Horlbeck MA, *et al.* 2016. Compact and highly active next-generation libraries for CRISPR-mediated gene repression and activation. *eLife* 5:e19760.
32 Eslami-Mossallam B, *et al.* 2022. A kinetic model predicts SpCas9 activity, improves off-target classification, and reveals the physical basis of targeting fidelity. *Nat Commun*. 13:1367.
33 Boyle EA, *et al.* 2017. High-throughput biochemical profiling reveals sequence determinants of dCas9 off-target binding and unbinding. *Proc Natl Acad Sci U S A*. 114:5461–5466.
34 Jones SK, *et al.* 2021. Massively parallel kinetic profiling of natural and engineered CRISPR nucleases. *Nat Biotechnol*. 39:84–93.
35 Bakalar MH, *et al.* 2018. Size-dependent segregation controls macrophage phagocytosis of antibody-opsonized targets. *Cell* 174:131–142.e13.
36 Morrissey MA, Kern N, Vale RD. 2020. CD47 ligation repositions the inhibitory receptor SIRPA to suppress integrin activation and phagocytosis. *Immunity* 53:290–302.e6.
37 Tsai RK, Discher DE. 2008. Inhibition of "self" engulfment through deactivation of myosin-II at the phagocytic synapse between human cells. *J Cell Biol*. 180:989–1003.
38 Suter EC, *et al.* 2021. Antibody:CD47 ratio regulates macrophage phagocytosis through competitive receptor phosphorylation. *Cell Rep*. 36:109587.
39 Dooling LJ, *et al.* 2023. Cooperative phagocytosis of solid tumours by macrophages triggers durable anti-tumour responses. *Nat Biomed Eng*. [Online ahead of print]. doi:10.1038/s41551-023-01031-3
40 Bruhns P. 2012. Properties of mouse and human IgG receptors and their contribution to disease models. *Blood* 119:5640–5649.
41 Nimmerjahn F, *et al.* 2010. FcγRIV deletion reveals its central role for IgG2a and IgG2b activity in vivo. *Proc Natl Acad Sci U S A*. 107: 19396–19401.
42 Li Y, *et al.* 2020. Vaccination with CD47 deficient tumor cells elicits an antitumor immune response in mice. *Nat Commun*. 11:581.
43 Aroldi F, Middleton MR. 2022. Long-term outcomes of immune checkpoint inhibition in metastatic melanoma. *Am J Clin Dermatol*. 23:331–338.
44 Waldman AD, Fritz JM, Lenardo MJ. 2020. A guide to cancer immunotherapy: from T cell basic science to clinical practice. *Nat Rev Immunol*. 20:651–668.
45 Lechner MG, *et al.* 2013. Immunogenicity of murine solid tumor models as a defining feature of in vivo behavior and response to immunotherapy. *J Immunother*. 36:477–489.

46 Arthur CM, *et al.* 2022. Clodronate inhibits alloimmunization against distinct red blood cell alloantigens in mice. *Transfusion* 62:948–953.
47 Zerra PE, *et al.* 2021. Marginal zone B cells mediate a CD4 T-cell–dependent extrafollicular antibody response following RBC transfusion in mice. *Blood* 138:706–721.
48 Cipponi A, *et al.* 2012. Neogenesis of lymphoid structures and antibody responses occur in human melanoma metastases. *Cancer Res.* 72:3997–4007.
49 Xu W, Banchereau J. 2014. The antigen presenting cells instruct plasma cell differentiation. *Front Immunol.* 4:504.